A comparative study of the magnetic induction heating properties of rare earth (RE = Y, La, Ce, Pr, Nd, Gd and Yb)-substituted magnesium–zinc ferrites

A comparative study of the magnetic induction heating properties of rare earth (RE = Y, La, Ce, Pr, Nd, Gd and Yb)-substituted magnesium–zinc ferrites

Fumie Hirosawa and Tomohiro Iwasaki*

Department of Chemical Engineering, Osaka Prefecture University, Sakai, Osaka 599–8531, Japan

*Corresponding author:
Tomohiro Iwasaki
E-mail: iwasaki@chemeng.osakafu-u.ac.jp
Postal address: 1–1 Gakuen-cho, Naka-ku, Sakai, Osaka, 599–8531, Japan
Tel: +81-72-254-9307, Fax: +81-72-254-9911

Abstract

Rare earth (RE)-substituted magnesium–zinc ferrite ($Mg_{0.5}Zn_{0.5}RE_xFe_{2-x}O_4$) nanoparticles with different RE elements (Y, La, Ce, Pr, Nd, Gd and Yb) and different RE contents (x = 0–0.1) were synthesized via coprecipitation of metal hydroxides as the precursor, followed by calcination. Their crystal structures were characterized by X-ray diffraction (XRD) analysis, confirming that the RE-substituted Mg–Zn ferrites had a single-phase spinel structure at low x values. However, the Ce-substituted ferrites contained CeO_2 as a byproduct. Scanning electron microscopy (SEM) showed that the particle diameters of the samples decreased from approximately 100 to 20 nm as x was increased regardless of the RE elements. The magnetic induction heating properties were evaluated using the intrinsic loss power (ILP) determined from the temperature rise profiles in an alternating magnetic field and the amplitude and frequency of the magnetic field. By using various RE elements, it was found that the increase in the magnetic moment of RE ions can increase the magnetization of ferrites, resulting in improvements in the ILP at low RE contents, except for Gd substitutions. The increase in RE content decreased the ILP due to reductions in crystallinity. The results suggest that the RE elements and contents can precisely control the magnetic induction heating properties, and RE-substituted Mg–Zn ferrite nanoparticles are promising candidates for magnetic hyperthermia applications.

Keywords

Magnesium–zinc ferrite; Rare earth substitution; Induction heating; Magnetic hyperthermia

1. Introduction

Spinel ferrites have been used for many applications, such as gas sensors [1],

microwave devices [2, 3], photocatalysts [4–8] and heating mediators for magnetic hyperthermia [9–14], due to their high chemical and thermal stabilities, high specific surface area, good magnetic properties and high electrical properties. These are strongly affected by the metal composition and crystallinity of ferrites [15–21]. To obtain ferrites with high performance, the partial substitution of Fe^{3+} ions in ferrites with rare earth (RE) ions has been used because of the larger ionic radii of RE^{3+} ions compared with Fe^{3+} ions, resulting in structural distortions and modifications of the magnetic and electrical properties [22–26]. Furthermore, substituting with different RE^{3+} ions may precisely control the properties of ferrites due to not only the monotonic change in ionic radii but also the periodical variation in the magnetic moments originating from the sequential filling of electrons in 4f shells [27]. Therefore, the effects of RE elements and RE contents on the properties of ferrites have been studied by many researchers [22–26, 28–34].

In recent years, among spinel ferrites, low-cost biocompatible soft magnetic magnesium–zinc ferrites ($Mg_yZn_{1-y}Fe_2O_4$; y = 0–1) have attracted much attention as heating mediators in magnetic hyperthermia treatments [35–37]. This is because of the good induction heating properties in an alternating (AC) magnetic field originating from excellent magnetic properties, such as magnetization and coercivity. For example, $Mg_{0.2}Zn_{0.8}Fe_2O_4$ exhibited good induction heating properties compared with conventional simple ferrites such as $CuFe_2O_4$, $MnFe_2O_4$, $NiFe_2O_4$, $SrFe_2O_4$ and $CoFe_2O_4$ [35, 38]. Moreover, Mg–Zn ferrites have good biocompatibility and have been studied as candidates for drug carriers for cancer treatments [39, 40] and as MRI contrast agents [41]. Due to the high performance of Mg–Zn ferrites, RE-substituted Mg–Zn ferrites can be candidates for a heating mediator in magnetic hyperthermia treatments. Therefore, some researchers have studied their magnetic properties [42–51]. Ladgaonkar et al. [46] assessed the variations in saturation magnetization in the amount of Fe^{3+} ions substituted with Nd^{3+} ions in Mg–Zn ferrites, demonstrating that the magnetization decreased with increasing Nd contents. Mukhtar et al. [47] examined the effects of the amount of Pr substitution in a Mg–Zn ferrite on the saturation magnetization and coercivity, confirming that the coercivity was improved by Pr substitution. For practical applications of RE-substituted Mg–Zn ferrites as a heating mediator in magnetic hyperthermia treatments, the induction heating properties should be precisely controlled. By substituting with various RE ions, the magnetic properties of ferrites can finely vary depending on the magnetic moments of the RE ions [27], which may lead to fine control of the heating properties. Therefore, it must be investigated systematically how various RE substitutions affect not only the magnetic properties but also the induction heating behaviors. Although we previously investigated the dependence of the induction heating properties on Gd substitution in Mg–Zn ferrites [52, 53], to the best of our knowledge, there are no comprehensive studies on the induction heating properties of RE-substituted Mg–Zn ferrites using various RE elements.

Therefore, to provide criteria for the preparation of Mg–Zn ferrites available for magnetic hyperthermia, RE-substituted Mg–Zn ferrites $Mg_yZn_{1-y}RE_xFe_{2-x}O_4$ (RE = Y, La, Ce,

Pr, Nd, Gd and Yb) were synthesized using various RE elements. We systematically examined the effects of the RE elements and the RE contents on the induction heating properties and discussed the role of RE substitution in the variation in induction heating properties toward the potential for easy and fine control of heating in magnetic hyperthermia treatments.

2. Experimental section

2.1 Synthesis

RE-substituted Mg–Zn ferrite ($Mg_yZn_{1-y}RE_xFe_{2-x}O_4$; RE = Y, La, Ce, Pr, Nd, Gd and Yb) nanoparticles with different compositions of x (x = 0, 0.015, 0.03, 0.06 and 0.1) were synthesized by calcination of a precursor consisting of metal hydroxides prepared via coprecipitation [52]. In this work, we used a Mg–Zn ferrite with y = 0.5 (i.e., $Mg_{0.5}Zn_{0.5}Fe_2O_4$) as a base material for its good induction heating properties [52]. Metal chloride solutions with a concentration of 0.1 M were individually prepared by dissolving $MgCl_2{\cdot}6H_2O$, $FeCl_3{\cdot}6H_2O$, $YCl_3{\cdot}6H_2O$, $LaCl_3{\cdot}7H_2O$, $CeCl_3{\cdot}7H_2O$, $NdCl_3{\cdot}6H_2O$, $GdCl_3{\cdot}6H_2O$, $YbCl_3{\cdot}6H_2O$ (FUJIFILM Wako Pure Chemical) and $PrCl_3{\cdot}7H_2O$ (KANTO CHEMICAL) in deionized water. In addition, a $ZnCl_2$ solution was prepared by dissolving $ZnCl_2$ (FUJIFILM Wako Pure Chemical) in 0.02 M HCl solution to completely dissolve $ZnCl_2$. Predetermined amounts of the metal chloride solutions corresponding to the RE elements and the RE contents were mixed and stirred for 10 min with a magnetic stirrer at room temperature. Subsequently, 1 M NaOH solution was quickly added to the solution under stirring, and a precipitation composed of a mixture of the metal hydroxides was formed. The final molar ratio of $OH^-/(Mg^{2+} + Zn^{2+} + RE^{3+} + Fe^{3+})$ in the resulting solution was fixed at 8/3, and the pH was approximately 12 regardless of the RE elements and contents. The solution was vigorously stirred for an additional 30 min. The precipitates were separated from the solution by centrifugation and washed with water several times to remove Na^+ and Cl^- ions. After that, the collected precipitates were dried at 383 K for 16 h. The obtained precursor was ground using a mortar and pestle and calcined at 1073 K for 5 h in air, and $Mg_{0.5}Zn_{0.5}RE_xFe_{2-x}O_4$ ferrites were formed.

2.2 Characterization

The phase evolution and crystallinity of the samples were evaluated using a powder X-ray diffractometer (XRD; XRD-6100, Shimadzu, Cu-Kα radiation, 30 kV, 30 mA) with a monochromator. The average crystallite size D was calculated via Scherrer's equation (Eq. (1)) using the diffraction data measured at $2\theta \approx 30.0°$, 35.4° and 62.4°, which corresponded to the (220), (311) and (440) planes, respectively.

$$D = K\lambda/(\beta\cos\theta) \quad (1)$$

where K is the Scherrer constant, β is the full width at half maximum (FWHM) of the peaks, λ is the X-ray wavelength (1.5418 Å), and θ is the diffraction angle. The a-axis lattice constant a

was also determined by Eq. (2) from the XRD data measured at the (220), (311) and (440) planes, and the average was calculated.

$$a = d_{hkl} (h^2 + k^2 + l^2)^{0.5} \quad (2)$$

where h, k and l are the Miller indices ($h\,k\,l$) and d_{hkl} is the interplanar spacing. The morphology was observed with a field emission scanning electron microscope (FE-SEM; JSM-6700F, JEOL, 18.0 kV). The elemental analysis by energy dispersive X-ray spectroscopy (EDX; Epsilon 1, Malvern Panalytical) was performed to determine the exact compositions of samples.

The induction heating properties of magnetic fluids consisting of the sample powder (5 mass%) and glycerol (FUJIFILM Wako Pure Chemical) were evaluated [52–54] using an AC magnetic field generator. It was composed of a radio frequency power source (T162-5723A, THAMWAY), an impedance matching box (T020-5723F, THAMWAY), and a solenoid coil (70 mm in inner diameter) with 21 turns of copper tube (4-mm outer diameter and 3-mm inner diameter). Cooling water flowed inside the copper tube. Briefly, 2.5 g of the magnetic fluid was charged in a glass test tube with an outer diameter of 15 mm. Although the nanoparticles were agglomerated during calcination, the aggregates were partly disintegrated in the fluid by ultrasonication prior to applying a magnetic field. After 10 min of sonication (20 kHz, 50 W) using a homogenizer (UH-50, SMT), the test tube was placed in the center of the coil. The temperature rise of the fluid in the AC magnetic field was measured with an optical fiber thermometer (FTI-10 with FOT-L-NS-967, FISO Technologies). The frequency f and amplitude H of the magnetic field were $f = 600$ kHz and $H = 5$ kA/m, respectively [52, 53]. Dutz and Hergt [55] suggest that $H \cdot f$ is less than 5×10^9 A/(m·s) as the biological safety limit. In this work, $H \cdot f = 3 \times 10^9$ A/(m·s), which satisfied the condition. The specific absorption rate (SAR) corresponding to the heat generation of the sample powder was determined using Eq. (3) according to the literature [35, 37, 56, 57].

$$\mathrm{SAR} = [\{mC_{\mathrm{pf}} + (1-m)C_{\mathrm{pg}}\}/m]\Delta t_{\mathrm{h}} \quad (3)$$

where m is the content of the sample powder in the fluid ($m = 0.05$) and C_{pf} and C_{pg} are the specific heat capacities of ferrites (0.64–0.68 J/(g·K) [58, 59]) and glycerol (2.43 J/(g·K) [54]), respectively. Δt_{h} is the elapsed time when the sample temperature reaches 45°C from 35°C, which is the effective temperature range for magnetic hyperthermia treatments [60, 61]. In this work, the intrinsic loss power (ILP) [62] was used to take into account the influences of amplitude and frequency of the magnetic field on the heating efficiency, expressed by

$$\mathrm{ILP} = \mathrm{SAR}/(H^2 f) \quad (4)$$

where H and f are the amplitude and frequency of the magnetic field, respectively.

3. Results and discussion

3.1 Characterization

Fig. 1 shows the XRD patterns of $Mg_{0.5}Zn_{0.5}RE_xFe_{2-x}O_4$ samples. Except for Ce-substituted Mg–Zn ferrites, the samples with low RE contents ($x \leq 0.03$) were confirmed to have a single-phase spinel structure. In contrast, when $x = 0.1$, Mg–Zn ferrites substituted with La, Pr and Nd contained rare earth orthoferrites, such as $LaFeO_3$, $PrFeO_3$ and $NdFeO_3$, respectively, as byproducts. Rare earth orthoferrites were observed in similar RE-substituted spinel ferrites, such as La-substituted Mg–Zn ferrites [63], Pr-substituted Mg ferrites [44], Pr-substituted Ni–Zn ferrites [64], Nd-substituted Mn–Zn ferrites [65] and Nd-substituted Mg–Cd ferrites [66]. Table 1 lists the actual RE compositions of samples except for the cases of Ce substitution. The RE compositions tended to coincide with the nominal values at low RE contents. In Ce-substituted Mg–Zn ferrites, cerium oxide (CeO_2) was contained as a byproduct because Ce^{3+} and Ce^{4+} ions can coexist in the samples [29]. The results demonstrated that our synthesis method can provide RE-substituted Mg–Zn ferrites at low RE contents except for Ce substitution and suggested that the formation of secondary phases leads to the reduction of the RE in the desired ferrite phases.

Table 1

Experimentally determined RE compositions in samples.

x (nominal)	Experimental values					
	Y	La	Pr	Nd	Gd	Yb
0.015	0.014	0.015	0.014	0.015	0.019	0.016
0.03	0.027	0.029	0.027	0.030	0.033	0.032
0.06	0.054	0.057	0.055	0.058	0.062	0.062
0.1	0.091	0.097	0.091	0.097	0.099	0.101

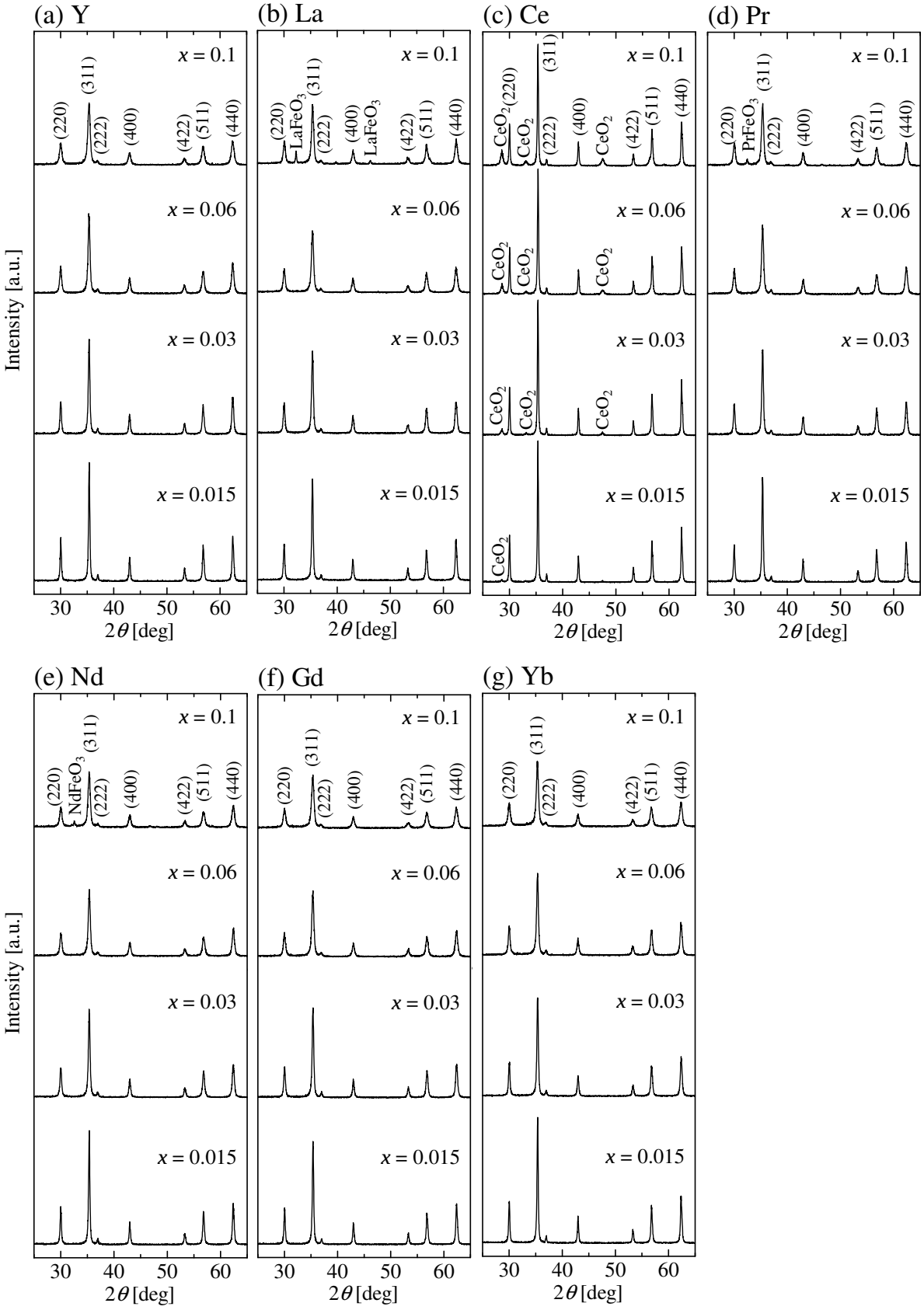

Fig. 1. XRD patterns of $Mg_{0.5}Zn_{0.5}RE_xFe_{2-x}O_4$ samples of RE = (a) Y, (b) La, (c) Ce, (d) Pr, (e) Nd, (f) Gd, and (g) Yb with $x = 0.015$–0.1.

As shown in Fig. 2, the lattice parameters a were strongly affected by the RE elements and contents. When small amounts of Fe^{3+} ions in Mg–Zn ferrites were substituted with Y^{3+}, Gd^{3+} and Yb^{3+} ions, the lattice parameters drastically decreased (Fig. 2a). This can be explained by the micro-strains in the internal grain region. According to Ateia et al. [29], the compression induced by the difference of the thermal expansion coefficient among the constituent elements and the lattice mismatch between the grain and the grain boundary phase can result in the generation of the micro-strains, which may decrease the lattice parameter. Subsequently, the lattice parameters gradually increased with the RE contents because the radii of RE^{3+} ions (Y^{3+} = 0.90 Å, Gd^{3+} = 0.94 Å and Yb^{3+} = 0.87 Å) were larger than that of Fe^{3+} ions (0.78 Å) [67]. Although the variations in the experimental data were relatively large due to the small changes in the lattice parameter, the results showed the significance of the non-monotonous changes of the lattice parameter, taking into account the range of variation. In contrast, the lattice parameters of the samples with RE = La, Ce, Pr and Nd decreased with the RE contents within x = 0–0.06 (Fig. 2b). This suggests that some of the RE^{3+} ions may not enter the spinel lattice but diffuse into the grain boundaries [63].

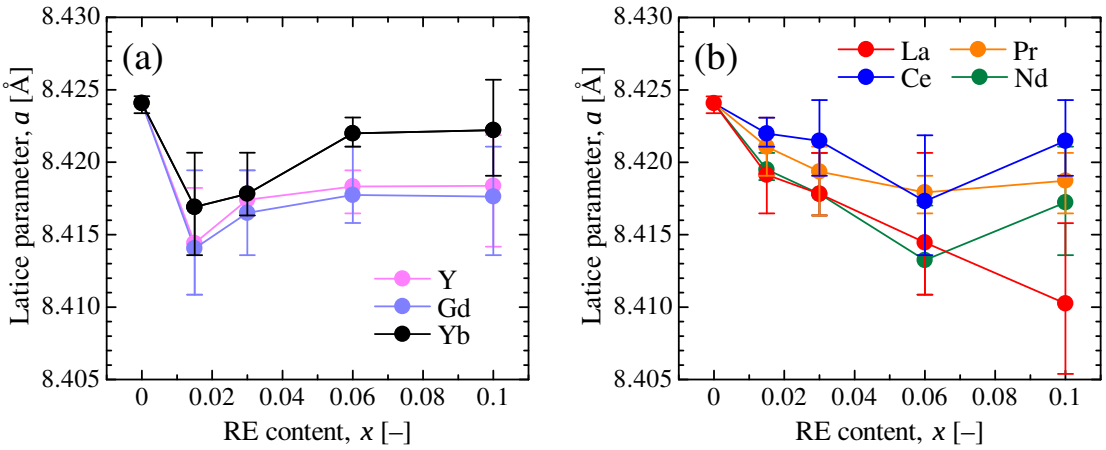

Fig. 2. Effect of RE elements on the variation in the a-axis lattice parameter with RE contents for RE = (a) Y, Gd and Yb, and (b) La, Ce, Pr and Nd.

Fig. 3 shows the effect of RE elements on the variations in average crystallite sizes D with the RE contents and the ionic radii of RE^{3+} ions at x = 0.015. The average crystallite sizes gradually decreased with increases in the RE contents except for Ce-substituted Mg–Zn ferrites (Fig. 3a). This is because of the inhibition of grain growth due to the larger binding energy of RE^{3+}–O^{2-} bonds than that of Fe^{3+}–O^{2-} bonds [68]. In Ce-substituted ferrites, a large amount of Ce^{3+} ions was spent to form CeO_2, resulting in higher crystallinities of the ferrites even at high Ce contents. As shown in Fig. 3b, the average crystallite sizes (except for Ce) at x = 0.015 decreased with increasing ionic radii of RE^{3+} ions, confirming that larger RE^{3+} ions more strongly inhibited grain growth. Regardless of x, similar tendencies of variations in D with the RE ionic radii were observed.

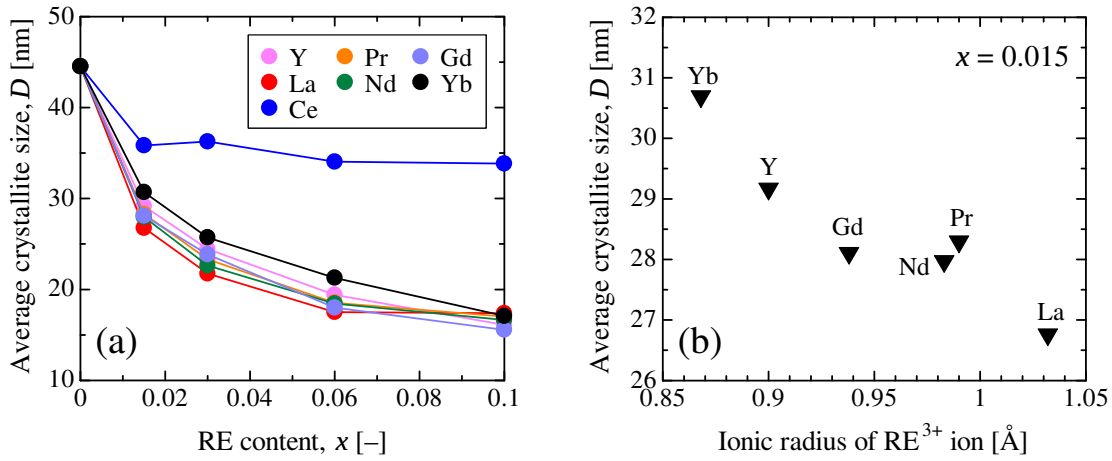

Fig. 3. Effect of RE elements on the variation in the average crystallite size with (a) RE contents and (b) ionic radii of RE^{3+} ions at $x = 0.015$.

Fig. 4 shows typical SEM images of $Mg_{0.5}Zn_{0.5}Yb_xFe_{2-x}O_4$ nanoparticles with $x = 0$, 0.03 and 0.1 as an example. The particle diameters decreased with RE contents ranging from approximately 100 to 20 nm. For other samples with different RE elements and contents, similar results were obtained. This may have been because RE^{3+} ions inhibit grain growth, as observed in similar ferrites such as Y-substituted Mg–Cd ferrites [69] and RE-substituted Co ferrites [22].

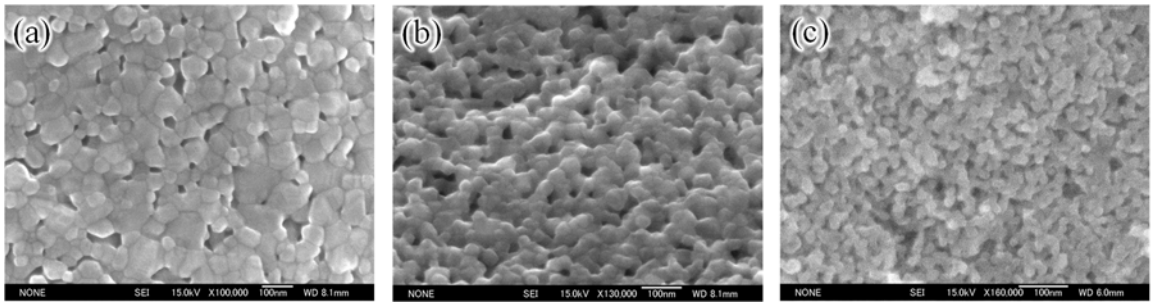

Fig. 4. Typical SEM images of $Mg_{0.5}Zn_{0.5}Yb_xFe_{2-x}O_4$ with x = (a) 0, (b) 0.03, and (c) 0.1.

3.2 Induction heating properties

Fig. 5 shows the typical temperature profiles of the magnetic fluids containing the $Mg_{0.5}Zn_{0.5}Yb_xFe_{2-x}O_4$ nanoparticles. The temperature of the magnetic fluids rapidly increased immediately after applying the magnetic field. In all samples, the magnetic fields were applied when the sample temperatures were approximately 30°C. Accordingly, for obtaining the SAR of the ferrites, the elapsed time Δt_h from the temperature rising from approximately 5 to 15 K were used (Fig. 5).

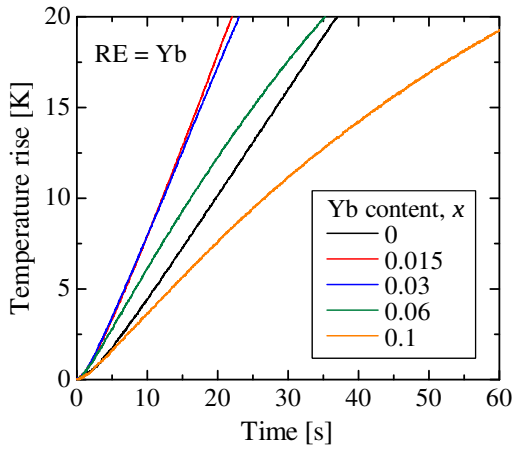

Fig. 5. Typical temperature profile curves of $Mg_{0.5}Zn_{0.5}Yb_xFe_{2-x}O_4$ with x = 0–0.1.

RE^{3+} ions have different magnetic moments [70, 71]. Thus, the variation in the magnetic moments can modify the magnetization of ferrites. This is because the Fe^{3+} ions (5 μ_B) in the octahedral B-sites can be replaced with the RE^{3+} ions (0–8 μ_B) in the Mg–Zn ferrites [47], which leads to variation in the induction heating properties [36, 37]. Fig. 6 illustrates the relationship between the ILP values and magnetic moments of the RE^{3+} ions at x = 0.015. Accordingly, the magnetization of Gd-substituted Mg–Zn ferrites may have increased and that of other RE-substituted Mg–Zn ferrites may have decreased, leading to increases in the ILP for RE = Gd and decreases for other RE elements. However, the ILP of the $Mg_{0.5}Zn_{0.5}Fe_2O_4$ (i.e., RE-free) sample was 1.80 nHm^2/kg-particle, confirming that the ILP values of RE-substituted ferrites increased regardless of the RE elements (Fig. 6). This may have been because small amounts of RE substitution can improve the magnetization and coercivity [26, 33, 68] due to the restraint of crystallization [27]. When various RE elements were used, the ILP values tended to increase at high magnetic moments of the RE^{3+} ions, possibly due to large magnetizations. However, despite the high magnetic moment of Gd^{3+} ion, the ILP of Gd-substituted Mg–Zn ferrites was smaller than that of other RE-substituted ferrites due to low coercivity, as observed in similar ferrites, such as RE-substituted Mn–Zn ferrites [26] and RE-substituted Ni–Zn ferrites [30]. Dutz and Hergt [55] suggest that typical ILP values suitable for heating are above 3 nHm^2/kg. Except for Ce substitution, the samples of x = 0.015 almost had an IPL value above this value, which implies that some RE-substituted Mg–Zn ferrites have an acceptable heating efficiency.

Fig. 7 shows the variations in ILP with the RE elements and contents. High ILP values were obtained when small amounts of Fe^{3+} ions were replaced with RE^{3+} ions. In contrast, when the RE contents were increased, the ILP gradually decreased except for the Ce-substituted ferrites, which had a similar tendency in the correlations of the average crystallite sizes and the RE contents (Fig. 3a). Fig. 8 shows the relationship between the average crystallite size D and the ILP of the ferrites. The ILP strongly depended on the average crystallite size D regardless of the RE elements because the improvement in crystallinity can increase the magnetization [72,

73]. The results suggested that the ILP of the RE-substituted Mg–Zn ferrites was strongly affected by the RE contents compared with the RE elements, and the RE contents and the RE elements could tune the induction heating widely and narrowly, respectively. Therefore, properly selecting the RE elements and adjusting the RE contents could lead to easy and fine control of the induction heating properties of RE-substituted Mg–Zn ferrites in magnetic hyperthermia treatments.

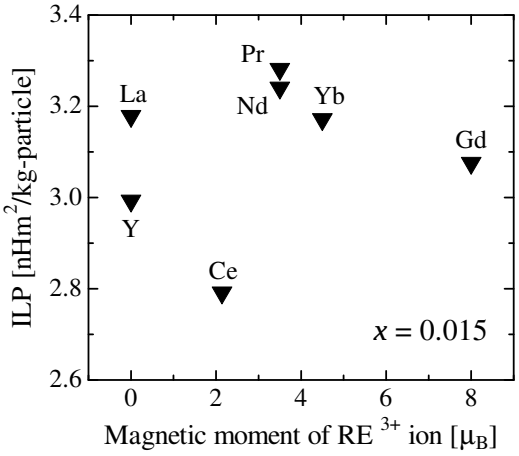

Fig. 6. Relationship between the ILP and magnetic moments of RE^{3+} ions at $x = 0.015$.

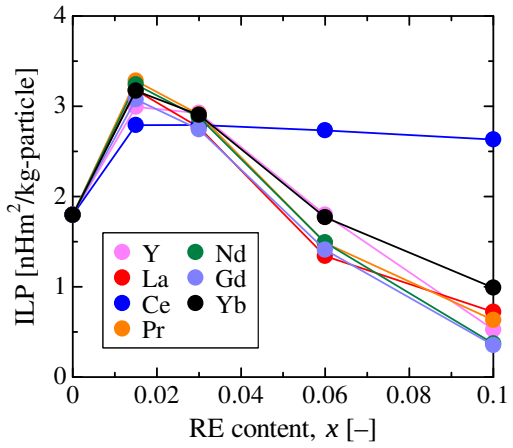

Fig. 7. Effect of RE elements on the variation in the ILP with RE contents.

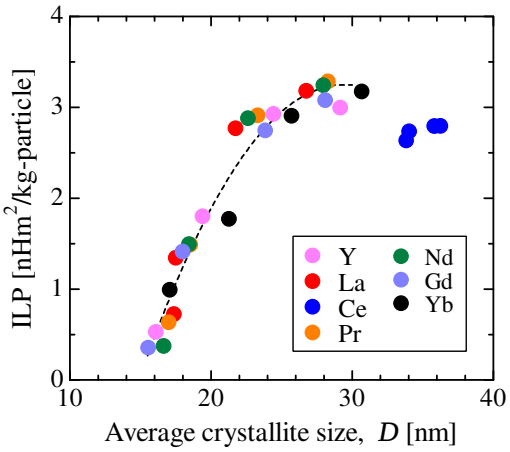

Fig. 8. Relationship between the ILP and average crystallite size.

4. Conclusion

RE-substituted Mg–Zn ferrite ($Mg_{0.5}Zn_{0.5}RE_xFe_{2-x}O_4$; RE = Y, La, Ce, Pr, Nd, Gd and Yb; x = 0–0.1) nanoparticles were prepared via coprecipitation of metal hydroxides as the precursors, followed by calcination in air. Except for Ce substitution, the synthesis process can successfully provide pure RE-substituted Mg–Zn ferrites with x ranging from 0 to 0.06. Some RE-substituted Mg–Zn ferrites (RE = La, Pr and Nd at x = 0.1) contained rare earth orthoferrites such as $LaFeO_3$, $PrFeO_3$ and $NdFeO_3$ as byproducts. In contrast, Ce-substituted Mg–Zn ferrites contained CeO_2 even when x was quite small. The lattice parameters and average crystallite sizes were found to depend strongly on the RE elements and the RE contents, resulting in variation in the magnetic induction heating properties. The ILP values of the RE-substituted Mg–Zn ferrites finely varied with the RE elements, possibly due to the differences in magnetic moments of the RE^{3+} ions. However, regardless of the RE elements, high ILP values were obtained at low RE contents, possibly due to improvements in the magnetization and coercivity of the ferrites. Subsequently, the ILP gradually decreased with the RE contents, except for Ce-substituted ferrites, due to a reduction in the average crystallite sizes. The use of various RE elements revealed that the induction heating properties of RE-substituted Mg–Zn ferrites can be controlled by adjusting the RE elements and contents. The results suggest that RE-substituted Mg–Zn ferrite nanoparticles are promising candidates as heating mediators which may lead to easy and fine control of heating in magnetic hyperthermia treatments for cancer therapy.

Acknowledgments

This work was supported by JSPS Research Fellowships for Young Scientists and JSPS KAKENHI Grant Number JP18J21860 and JP19K05216.

References

[1] A. Šutka, K.A. Gross, Spinel ferrite oxide semiconductor gas sensors, Sensor. Actuat. B: Chem. 222 (2016) 95–105. https://doi.org/10.1016/j.snb.2015.08.027

[2] J.D. Adam, L.E. Davis, G.F. Dionne, E.F. Schloemann, S.N. Stitzer, Ferrite devices and materials, IEEE T. Microw. Theory Techni. 50 (2002) 721–737. https://ieeexplore.ieee.org/stamp/stamp.jsp?arnumber=989957

[3] V.G. Harris, A. Geiler, Y. Chen, S.D. Yoon, M. Wu, A. Yang, Z. Chen, P. He, P.V. Parimi, X. Zuo, C.E. Patton, M. Abe, O. Acher, C. Vittoria, Recent advances in processing and applications of microwave ferrites, J. Magn. Magn. Mater. 321 (2009) 2035–2047. https://doi.org/10.1016/j.jmmm.2009.01.004

[4] M. Amiri, K. Eskandari, M. Salavati-Niasari, 2019. Magnetically retrievable ferrite nanoparticles in the catalysis application, Adv. Colloid Interfac. Sci. 271, 101982. https://doi.org/10.1016/j.cis.2019.07.003

[5] K.K. Kefeni, B.B. Mamba, T.A.M. Msagati, Application of spinel ferrite nanoparticles in water and wastewater treatment: a review, Sep. Purif. Technol. 188 (2017) 399–422. https://doi.org/10.1016/j.seppur.2017.07.015

[6] K.K. Kefeni, B.B. Mamba, 2020. Photocatalytic application of spinel ferrite nanoparticles and nanocomposites in wastewater treatment: review, SM&T, 23, e00140. https://doi.org/10.1016/j.susmat.2019.e00140

[7] M.I.A.A. Maksoud, A.M. Elgarahy, C. Farrell, A.H. Al-Muhtaseb, D.W. Rooney, A.I. Osman, 2020. Insight on water remediation application using magnetic nanomaterials and biosorbents, Coordin. Chem. Rev. 403, 213096. https://doi.org/10.1016/j.ccr.2019.213096

[8] D.H.K. Reddy, Y. Yun, Spinel ferrite magnetic adsorbents: alternative future materials for water purification?, Coordin. Chem. Rev. 315 (2016) 90–111. https://doi.org/10.1016/j.ccr.2016.01.012

[9] E.C. Abenojar, S. Wickramasinghe, J. Bas-Concepcion, A.C.S. Samia, Structural effects on the magnetic hyperthermia properties of iron oxide nanoparticles, Prog. Nat. Sci.: Mater. Int. 26 (2016) 440–448. https://doi.org/10.1016/j.pnsc.2016.09.004

[10] Z. Hedayatnasab, F. Abnisa, W.M.A.W. Daud, Review on magnetic nanoparticles for magnetic nanofluid hyperthermia application, Mater. Design 123 (2017) 174–196. https://doi.org/10.1016/j.matdes.2017.03.036

[11] K.K. Kefeni, T.A.M. Msagati, T.T.I. Nkambule, B.B. Mamba, 2020. Spinel ferrite nanoparticles and nanocomposites for biomedical applications and their toxicity, Mat. Sci. Eng. C 107, 110314. https://doi.org/10.1016/j.msec.2019.110314

[12] J. Mohapatra, M. Xing, J.P. Liu, 2019. Inductive thermal effect of ferrite magnetic nanoparticles, Materials 12, 3208. https://doi.org/10.3390/ma12193208

[13] S. Laurent, S. Dutz, U.O. Häfeli, M. Mahmoudi, Magnetic fluid hyperthermia: focus on superparamagnetic iron oxide nanoparticles, Adv. Colloid Interfac. Sci. 166 (2011) 8–23. https://doi.org/10.1016/j.cis.2011.04.003

[14] Z. Shaterabadi, G. Nabiyouni, M. Soleymani, Physics responsible for heating efficiency and self-controlled temperature rise of magnetic nanoparticles in magnetic

hyperthermia therapy, Prog. Biophys. Mol. Bio. 133 (2018) 9–19. https://doi.org/10.1016/j.pbiomolbio.2017.10.001

[15] D. Damma, D. Jampaiah, A. Welton, P. Boolchand, A. Arvanitis, J. Dong, P.G. Smirniotis, Effect of Nb modification on the structural and catalytic property of Fe/Nb/M (M = Mn, Co, Ni, and Cu) catalyst for high temperature water-gas shift reaction, Catal. Today, in press. https://doi.org/10.1016/j.cattod.2019.02.029

[16] F. Sharifianjazi, M. Moradi, N. Parvin, A. Nemati, A.J. Rad, N. Sheysi, A. Abouchenari, A. Mohammadi, S. Karbasi, Z. Ahmadi, A. Esmaeilkhanian, M. Irani, A. Pakseresht, S. Sahmani, M.S. Asl, Magnetic $CoFe_2O_4$ nanoparticles doped with metal ions: a review, Ceram. Int. 46 (2020) 18391–18412. https://doi.org/10.1016/j.ceramint.2020.04.202

[17] D.H. Taffa, R. Dillert, A.C. Ulpe, K.C.L. Bauerfeind, T. Bredow, D.W. Bahnemann, M. Wark, 2016. Photoelectrochemical and theoretical investigations of spinel type ferrites ($M_xFe_{3-x}O_4$) for water splitting: a mini-review, J. Photonics Energy 7, 012009. https://doi.org/10.1117/1.JPE.7.012009

[18] N. Fortas, A. Belkahla, S. Ouyahia, J. Dhahri, E.K. Hlil, K. Taibi, 2020. Effect of Ni substitution on the structural, magnetic and magnetocaloric properties of $Zn_{0.5-x}Ni_xMg_{0.5}Fe_2O_4$ (x = 0, 0.125 and 0.250) ferrites, Solid State Sci. 101, 106137. https://doi.org/10.1016/j.solidstatesciences.2020.106137

[19] A. Lassoued, J.F. Li, 2020. Magnetic and photocatalytic properties of Ni–Co ferrites, Solid State Sci. 104, 106199. https://doi.org/10.1016/j.solidstatesciences.2020.106199

[20] Z. Klencsár, G. Tolnai, L. Korecz, I. Sajó, P. Németh, J. Osán, S. Mészáros, E. Kuzmann, Cation distribution and related properties of $Mn_xZn_{1-x}Fe_2O_4$ spinel nanoparticles, Solid State Sci. 24 (2013) 90–100. https://doi.org/10.1016/j.solidstatesciences.2013.07.010

[21] M.A. Ahmed, S.I. El-Dek, I.M. El-Kashef, N. Helmy, Structural and magnetic properties of nano-crystalline Ag^+ doped $NiFe_2O_4$, Solid State Sci. 13 (2011) 1176–1179. https://doi.org/10.1016/j.solidstatesciences.2010.11.002

[22] G. Bulai, L. Diamandescu, I. Dumitru, S. Gurlui, M. Feder, O.F. Caltun, Effect of rare earth substitution in cobalt ferrite bulk materials, J. Magn. Magn. Mater. 390 (2015) 123–131. https://doi.org/10.1016/j.jmmm.2015.04.089

[23] S.M. Peymani-Motlagh, A. Sobhani-Nasab, M. Rostami, H. Sobati, M. Eghbali-Arani, M. Fasihi-Ramandi, M.R. Ganjali, M. Rahimi-Nasrabadi, Assessing the magnetic, cytotoxic and photocatalytic influence of incorporating Yb^{3+} or Pr^{3+} ions in cobalt–nickel ferrite, J. Mater. Sci.: Mater. El. 30 (2019) 6902–6909. https://doi.org/10.1007/s10854-019-01005-9

[24] M.M. El-Sayed, Rare-earth substitution effect on the quality of Mg–Ti ferrite, Ceram. Int. 33 (2007) 413–418. https://doi.org/10.1016/j.ceramint.2005.09.025

[25] X. Wu, Z. Ding, N. Song, L. Li, W. Wang, Effect of the rare-earth substitution on the

structural, magnetic and adsorption properties in cobalt ferrite nanoparticles, Ceram. Int. 42 (2016) 4246–4255. https://doi.org/10.1016/j.ceramint.2015.11.100

[26] M. Yousaf, M.N. Akhtar, B. Wang, A. Noor, Preparations, optical, structural, conductive and magnetic evaluations of RE's (Pr, Y, Gd, Ho, Yb) doped spinel nanoferrites, Ceram. Int. 46 (2020) 4280–4288. https://doi.org/10.1016/j.ceramint.2019.10.149

[27] B. Zhou, Y. Zhang, C. Liao, C. Yan, L. Chen, S. Wang, Rare-earth-mediated magnetism and magneto-optical Kerr effects in nanocrystalline $CoFeMn_{0.9}RE_{0.1}O_4$ thin films, J. Magn. Magn. Mater. 280 (2004) 327–333. https://doi.org/10.1016/j.jmmm.2004.03.031

[28] A.M.A.E. Ata, M.K. El-Nimr, S.M. Attia, D. El-Kony, A.H. Al-Hammadi, Studies of AC electrical conductivity and initial magnetic permeability of rare-earth-substituted Li–Co ferrites, J. Magn. Magn. Mater. 297 (2006) 33–43. https://doi.org/10.1016/j.jmmm.2005.01.085

[29] E.E. Ateia, M.A. Ahmed, L.M. Salah, A.A. El-Gamal, Effect of rare earth oxides and La^{3+} ion concentration on some properties of Ni–Zn ferrites, Physica B Cond. Mat. 445 (2014) 60–67. https://doi.org/10.1016/j.physb.2014.03.094

[30] G.V. Bazuev, O.I. Gyrdasova, S.I. Novikov, A.Y. Kuznetsov, Synthesis, structure, and magnetic properties of rare-earth-doped $Ni_{0.75}Zn_{0.25}Fe_2O_4$ nickel zinc ferrite, Inorg. Mater. 52 (2016) 932–938. https://doi.org/10.1134/S0020168516090028

[31] F. Cheng, J. Jia, Z. Xu, B. Zhou, C. Liao, C. Yan, L. Chen, H. Zhao, Microstructure, magnetic, and magneto-optical properties of chemical synthesized Co–RE (RE = Ho, Er, Tm, Yb, Lu) ferrite nanocrystalline films, J. Appl. Phys. 86 (1999) 2727–2732. https://doi.org/10.1063/1.371117

[32] A.A.H. El-Bassuony, A Comparative study of physical properties of Er and Yb nanophase ferrite for industrial application, J. Supercond. Nov. Magn. 31 (2018) 2829–2840. https://doi.org/10.1007/s10948-017-4543-1

[33] C. Virlan, G. Bulai, O.F. Caltun, R. Hempelmann, A. Pui, Rare earth metals' influence on the heat generating capability of cobalt ferrite nanoparticles, Ceram. Int. 42 (2016) 11958–11965. https://doi.org/10.1016/j.ceramint.2016.04.121

[34] U.B. Tumberphale, S.S. Jadhav, S.D. Raut, P.V. Shinde, S. Sangle, S.F. Shaikh, A.M. Al-Enizi, M. Ubaidullah, R.S. Mane, S.K. Gore, 2020. Tailoring ammonia gas sensing performance of La^{3+}-doped copper cadmium ferrite nanostructures, Solid State Sci. 100, 106089. https://doi.org/10.1016/j.solidstatesciences.2019.106089

[35] H.M. El-Sayed, I.A. Ali, A. Azzam, A.A. Sattar, Influence of the magnetic dead layer thickness of Mg-Zn ferrites nanoparticle on their magnetic properties, J. Magn. Magn. Mater. 424 (2017) 226–232. https://doi.org/10.1016/j.jmmm.2016.10.049

[36] H. Liu, A. Li, X. Ding, F. Yang, K. Sun, Magnetic induction heating properties of $Mg_{1-x}Zn_xFe_2O_4$ ferrites synthesized by co-precipitation method, Solid State Sci. 93 (2019) 101–108. https://doi.org/10.1016/j.solidstatesciences.2019.05.005

[37] P.Y. Reyes-Rodríguez, D.A. Cortés-Hernández, J.C. Escobedo-Bocardo, J.M. Almanza-Robles, H.J. Sánchez-Fuentes, A. Jasso-Terán, L.E.D. León-Prado, J. Méndez-Nonell, G.F. Hurtado-López, Structural and magnetic properties of Mg-Zn ferrites ($Mg_{1-x}Zn_xFe_2O_4$) prepared by sol-gel method, J. Magn. Magn. Mater. 427 (2017) 268–271. https://doi.org/10.1016/j.jmmm.2016.10.078

[38] T. Maehara, K. Konishi, T. Kamimori, H. Aono, H. Hirazawa, T. Naohara, S. Nomura, H. Kikkawa, Y. Watanabe, K. Kawachi, Selection of ferrite powder for thermal coagulation therapy with alternating magnetic field, J. Mater. Sci. 40 (2005) 135–138. https://doi.org/10.1007/s10853-005-5698-x

[39] S. Kanagesan, M. Hashim, S. Tamilselvan, N.B. Alitheen, I. Ismail, G. Bahmanrokh, 2013. Cytotoxic effect of nanocrystalline $MgFe_2O_4$ particles for cancer cure, J. Nanomater. 2013, 865024. http://dx.doi.org/10.1155/2013/865024

[40] S. Kanagesan, M. Hashim, S.A.B. Aziz, I. Ismail, S. Tamilselvan, N.B. Alitheen, M.K. Swamy, B.P.C. Rao, 2016. Evaluation of antioxidant and cytotoxicity activities of copper ferrite ($CuFe_2O_4$) and zinc ferrite ($ZnFe_2O_4$) nanoparticles synthesized by sol-gel self-combustion method, Appl. Sci. 6, 184. https://doi.org/10.3390/app6090184

[41] N. Alghamdi, J. Stroud, M. Przybylski, J. Żukrowski, A.C. Hernandez, J.M. Brown, J.H. Hankiewicz, Z. Celinski, 2020. Structural, magnetic and toxicity studies of ferrite particles employed as contrast agents for magnetic resonance imaging thermometry, J. Magn. Magn. Mater. 497, 165981. https://doi.org/10.1016/j.jmmm.2019.165981

[42] K. Bibi, I. Ali, M.T. Farid, A. Mahmood, S.M. Ramay, K. Ali, Electric and dielectric properties of ytterbium substituted spinel ferrites, J. Mater. Sci.: Mater. El. 29 (2018) 3744–3750. https://doi.org/10.1007/s10854-017-8308-1

[43] A.S. Elkady, S.I. Hussein, M.M. Rashad, Structural and magnetic properties of Gd^{3+} ion substituted magnesium ferrite nanopowders, J. Magn. Magn. Mater. 385 (2015) 70–76. https://doi.org/10.1016/j.jmmm.2015.03.008

[44] M.T. Farid, I. Ahmad, M. Kanwal, G. Murtaza, I. Ali, S.A. Khan, The role of praseodymium substituted ions on electrical and magnetic properties of Mg spinel ferrites, J. Magn. Magn. Mater. 428 (2017) 136–143. https://doi.org/10.1016/j.jmmm.2016.12.031

[45] H.A. Hejase, S.S. Hayek, S.M. Qadri, Y.S. Haik, Self-controlled hyperthermia characteristics of ZnGdFe nanoparticles, IEEE Trans. Magn. 48 (2012) 2430–2439. https://doi.org/10.1109/TMAG.2012.2196284

[46] B.P. Ladgaonkar, C.B. Kolekar, A.S. Vaingankar, Magnetization and initial permeability studies of Nd^{3+} substituted Zn–Mg ferrite system, Bull. Mater. Sci. 22 (1999) 917–920. https://doi.org/10.1007/BF02745553

[47] M.W. Mukhtar, M. Irfan, I. Ahmad, I. Ali, M.N. Akhtar, M.A. Khan, G. Abbas, M.U. Rana, A. Ali, M. Ahmad, Synthesis and properties of Pr-substituted MgZn ferrites for core materials and high frequency applications, J. Magn. Magn. Mater. 381 (2015)

173–178. https://doi.org/10.1016/j.jmmm.2014.12.072

[48] P. Raja, T. Yadavalli, D. Ravi, H.A. Therese, C. Ramasamy, Y. Hayakawa, Synthesis and magnetic properties of gadolinium substituted zinc ferrites, Mater. Lett. 188 (2017) 406–408. https://doi.org/10.1016/j.matlet.2016.11.083

[49] R. Tholkappiyan, K. Vishista, Combustion synthesis of Mg–Er ferrite nanoparticles: cation distribution and structural, optical, and magnetic properties, Mat. Sci. Semicon. Proc. 40 (2015) 631–642. https://doi.org/10.1016/j.mssp.2015.06.076

[50] M. Vucinic-Vasic, E.S. Bozin, L. Bessais, G. Stojanovic, U. Kozmidis-Luburic, M. Abeykoon, B. Jancar, A. Meden, A. Kremenovic, B. Antic, Thermal evolution of cation distribution/crystallite size and their correlation with the magnetic state of Yb-substituted zinc ferrite nanoparticles, J. Phys. Chem. C 117 (2013) 12358−12365. https://doi.org/10.1021/jp403459t

[51] A. Yao, F. Ai, D. Wang, W. Huang, X. Zhang, Synthesis, characterization and in vitro cytotoxicity of self-regulating magnetic implant material for hyperthermia application, Mater. Sci. Eng. C 29 (2009) 2525–2529. https://doi.org/10.1016/j.msec.2009.07.021

[52] F. Hirosawa, T. Iwasaki, S. Watano, Synthesis and magnetic induction heating properties of Gd-substituted Mg–Zn ferrite nanoparticles, Appl. Nanosci. 7 (2017) 209–214. https://doi.org/10.1007/s13204-017-0566-y

[53] F. Hirosawa, T. Iwasaki, S. Watano, 2016. Induction heating properties of Gd-substituted Mg–Zn ferrite nanoparticles in an AC magnetic field, Proceedings of 9th Pacific Rim international conference on advanced materials and processing (PRICM9), Kyoto, Japan, PS6-17.

[54] I.S. Smolkova, N.E. Kazantseva, H. Parmar, V. Babayan, P. Smolka, P. Saha, Correlation between coprecipitation reaction course and magneto-structural properties of iron oxide nanoparticles, Mater. Chem. Phys. 155 (2015) 178–190. https://doi.org/10.1016/j.matchemphys.2015.02.022

[55] S. Dutz, R. Hergt, Magnetic nanoparticle heating and heat transfer on a microscale: basic principles, realities and physical limitations of hyperthermia for tumour therapy, Int. J. Hyperthermia 29 (2013) 790–800. https://doi.org/10.3109/02656736.2013.822993

[56] I. Khishigdemberel, E. Uyanga, H. Hirazawa, B. Enkhmend, I.A. Bobrikov, D. Sangaa, T. Kiseleva, 2020. Structural, infrared and magnetic properties of $MgAl_xFe_{2-x}O_4$ compounds: effect of the preparation methods and Al substitution, Solid State Sci. 109, 106400. https://doi.org/10.1016/j.solidstatesciences.2020.106400

[57] O.V. Yelenich, S.O. Solopan, J.M. Greneche, A.G. Belous, Synthesis and properties MFe_2O_4 (M = Fe, Co) nanoparticles and core–shell structures, Solid State Sci. 46 (2015) 19–26. https://doi.org/10.1016/j.solidstatesciences.2015.05.011

[58] S. Hajarpour, K. Gheisari, A.H. Raouf, Characterization of nanocrystalline $Mg_{0.6}Zn_{0.4}Fe_2O_4$ soft ferrites synthesized by glycine-nitrate combustion process, J. Magn. Magn. Mater. 329 (2013) 165–169.

https://doi.org/10.1016/j.jmmm.2012.10.023
[59] S. Klemme, M. Ahrens, Low-temperature heat capacity of magnesioferrite ($MgFe_2O_4$), Phys. Chem. Miner. 32 (2005) 374–378. https://doi.org/10.1007/s00269-005-0003-8
[60] Z. Ling-Yun, L. Jia-Yi, O. Wei-Wei, L. Dan-Ye, L. Li, L. Li-Ya, T. Jin-Tian, 2013. Magnetic-mediated hyperthermia for cancer treatment: research progress and clinical trials, Chin. Phys. B 22, 108104. http://dx.doi.org/10.1088/1674-1056/22/10/108104
[61] B. Thiesen, A. Jordan, Clinical applications of magnetic nanoparticles for hyperthermia, Int. J. Hyperthermia 24 (2008) 467–474. https://doi.org/10.1080/02656730802104757
[62] M. Kallumadil, M. Tada, T. Nakagawa, M. Abe, P. Southern, Q.A. Pankhurst, Suitability of commercial colloids for magnetic hyperthermia, J. Magn. Magn. Mater. 321 (2009) 1509–1513. https://doi.org/10.1016/j.jmmm.2009.02.075
[63] I. Ahmad, M.T. Farid, R. Kousar, S.B. Niazi, Structural and electrical properties of lanthanum substituted spinel ferrites, WASJ 22 (2013) 796–801. http://www.idosi.org/wasj/wasj22(6)13/6.pdf
[64] B. Yan, P. Gao, Z. Lu, R. Ma, E.V. Rebrov, H. Zheng, Y. Gao, Effect of Pr^{3+} substitution on the microstructure, specific surface area, magnetic properties and specific heating rate of $Ni_{0.5}Zn_{0.5}Pr_xFe_{2-x}O_4$ nanoparticles synthesized via sol–gel method, J. Alloy. Compd. 639 (2015) 626–634. https://doi.org/10.1016/j.jallcom.2015.03.211
[65] P. Thakur, R. Sharma, M. Kumar, S.C. Katyal, P.B. Barman, V. Sharma, P. Sharma, Structural, morphological, magnetic and optical study of co-precipitated Nd^{3+} doped Mn-Zn ferrite nanoparticles, J. Magn. Magn. Mater. 479 (2019) 317–325. https://doi.org/10.1016/j.jmmm.2019.02.048
[66] S.R. Bhongale, H.R. Ingawale, T.J. Shinde, P.N. Vasambekar, Effect of Nd^{3+} substitution on structural and magnetic properties of Mg–Cd ferrites synthesized by microwave sintering technique, J. Rare Earth. 36 (2018) 390–397. https://doi.org/10.1016/j.jre.2017.11.003
[67] R.D. Shannon, Revised effective ionic radii and systematic studies of interatomic distances, in halides and chalcogenides, Acta Cryst. A 32 (1976) 751–767.
[68] D. Li, Y. Sun, Y. Xu, H. Ge, Q. Wu, C. Yan, Effects of Dy^{3+} substitution on the structural and magnetic properties of $Ni_{0.5}Zn_{0.5}Fe_2O_4$ nanoparticles prepared by a sol-gel self-combustion method, Ceram. Int. 41 (2015) 4581–4589. https://doi.org/10.1016/j.ceramint.2014.11.156
[69] A.B. Gadkari, T.J. Shinde, P.N. Vasambekar, Structural analysis of Y^{3+}-doped Mg–Cd ferrites prepared by oxalate co-precipitation method, Mater. Chem. Phys. 114 (2009) 505–510. https://doi.org/10.1016/j.matchemphys.2008.11.011
[70] B. Shahbahrami, S.M. Rabiee, R. Shidpoor, An overview of cobalt ferrite core-shell nanoparticles for magnetic hyperthermia applications, ACERP 6 (2020) 1–15. https://dx.doi.org/10.30501/acp.2020.105923
[71] T. Muranaka, J. Akimitsu, Thermodynamic properties of ferromagnetic Ce-compound,

$CeAgAl_3$, Physica C: Supercond. Appl. 460–462 (2007) 688–690. https://doi.org/10.1016/j.physc.2007.03.127

[72] C. Choodamani, G.P. Nagabhushana, B. Rudraswamy, G.T. Chandrappa, Thermal effect on magnetic properties of Mg-Zn ferrite nanoparticles, Mater. Lett. 116 (2014) 227–230. https://doi.org/10.1016/j.matlet.2013.11.024

[73] C. Murugesan, G. Chandrasekaran, Enhanced electrical and magnetic properties of annealed magnesium ferrite nanoparticles, J. Supercond. Nov. Magn. 28 (2015) 3607–3615. https://doi.org/10.1007/s10948-015-3198-z